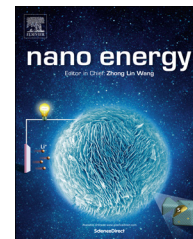




Available online at [www.sciencedirect.com](http://www.sciencedirect.com)

ScienceDirect

journal homepage: [www.elsevier.com/locate/nanoenergy](http://www.elsevier.com/locate/nanoenergy)



RAPID COMMUNICATION

# Blow-driven triboelectric nanogenerator as an active alcohol breath analyzer



Zhen Wen<sup>a,b,1</sup>, Jun Chen<sup>a,1</sup>, Min-Hsin Yeh<sup>a,1</sup>, Hengyu Guo<sup>a</sup>,  
Zhaoling Li<sup>a</sup>, Xing Fan<sup>a</sup>, Tiejun Zhang<sup>a</sup>, Liping Zhu<sup>b,\*</sup>,  
Zhong Lin Wang<sup>a,c,\*</sup>

<sup>a</sup>*School of Materials Science and Engineering, Georgia Institute of Technology, Atlanta, GA 30332-0245, United States*

<sup>b</sup>*State Key Laboratory of Silicon Materials, School of Materials Science & Engineering, Cyrus Tang Center for Sensor Materials and Applications, Zhejiang University, Hangzhou 310027, China*

<sup>c</sup>*Beijing Institute of Nanoenergy and Nanosystems, Chinese Academy of Sciences, Beijing 100083, China*

Received 11 May 2015; received in revised form 7 June 2015; accepted 11 June 2015

Available online 23 June 2015

## KEYWORDS

Triboelectrification;  
Blow-driven;  
Self-powered;  
Alcohol;  
Gas sensing

## Abstract

Gas sensing is an important technology that is widely used in life science, security and environmental protection. In this work, we introduced a fundamentally new working principle in the gas sensing field by fabricating a blow-driven triboelectric nanogenerator (BD-TENG). By using the electricity generated via mouth blowing, the induced voltage across the sensor holds a proportional relationship with the breathed-out alcohol concentration regardless the blow speed and quality air-flow. The as-developed BD-TENG, acting as an active alcohol breath analyzer, is featured as high detection gas response of  $\sim 34$  under an optimized sensor working temperature, fast response time of 11 s as well as a fast recovery of 20 s. Moreover, the device shows outstanding capability of selectivity anti-interference for alcohol detection. In addition, fabricated of common polymer materials, the reported breath analyzer is still light-weight and cost-effective. The BD-TENG based alcohol detector not only presents a new principle in the field of gas sensing, but also greatly advances the applicability of TENGs as self-powered active sensors.

© 2015 Published by Elsevier Ltd.

\*Corresponding authors at: School of Materials Science and Engineering, Georgia Institute of Technology, Atlanta, GA 30332-0245, United States.

E-mail addresses: [zlp1@zju.edu.cn](mailto:zlp1@zju.edu.cn) (L. Zhu), [zhong.wang@mse.gatech.edu](mailto:zhong.wang@mse.gatech.edu) (Z.L. Wang).

<sup>1</sup>These authors contributed equally to this work.

## Introduction

Gas sensing is widely used for monitoring the concentration and species of ambient gases, especially for the detection of toxic or explosive gases [1-4]. Ethanol, as a common volatile chemical in many industrial productions, its detection is vital for safety and drunk driving testing [5-8]. Various approaches have been proposed for alcohol detection, including gas chromatography, infrared spectroscopy, colorimetric sensor, fuel cells-based sensors and semiconductor-based sensors [9-13]. Widespread usage of these techniques is likely to be shadowed by possible limitations, such as high-cost, structure complexity, requirements of high-quality materials and reliance on external power source.

In this regard, we report a blow-driven triboelectric nanogenerator (BD-TENG) based gas sensor for active alcohol detection. Based on a coupling of contact electrification and electrostatic induction [14-24], the as-developed alcohol sensor can convert energy from air flow to power itself, the delivered voltage holds a proportional relationship with the breathed-out alcohol concentration in a wide sensing range of 10 to 200 ppm regardless the blowing speed and quality of blown air. With a good response/recovery kinetics (11 s and 20 s), the BD-TENG based alcohol gas sensor exhibits a high gas response of  $\sim 34$  to 100 ppm alcohol under an optimized working temperature of 160 °C. Moreover, via testing with other similar gases, the BD-TENG based device still shows outstanding selectivity for alcohol detection. In addition, fabricated using common polymer materials, the as-developed breath analyzer is lightweight, cost-effective and easy fabrication. Given a collection of exceptional properties resulting from its distinctive working mechanism and novel structural design, the BD-TENG based alcohol detector not only launches a new working principle in the field of gas sensing, but also greatly advances the applicability of TENGs as self-powered active sensors.

## Experimental

### Fabrication of a blow-driven triboelectric nanogenerator

The BD-TENG mainly consists of three parts: a stator, a rotator and a soft elastic. First, for the stator, acrylic sheet with thickness of 1/16 inch was shaped by a laser cutter (PLS6.75, Universal Laser Systems) to form the disk substrate. Then, electrodes with complementary patterns have been deposited onto the substrate by physical vapor deposition (PVD). And the copper electrodes were separated by laser-cutter-defined fine trenches in between. Second, for the rotator, cut a disc-shaped acrylic sheet as a substrate with a diameter of 5 cm using the laser cutter. And then a layer of fluorinated ethylene propylene (FEP) ( $\sim 50 \mu\text{m}$ ), first tailored into an eighteen-segment structure, was aligned onto the substrate as one of the triboelectric surface. Connect two lead wires respectively to the two sets of electrodes. A soft elastic was employed as a spacer between the rotator and the stator.

### Fabrication of nanowires array on FEP surface

A 50  $\mu\text{m}$  thick FEP thin film was washed with menthol, isopropyl alcohol, and deionized water, consecutively, and

then dry with compressed nitrogen gas. Using a DC sputter, coat a 10 nm thick layer of Au onto the FEP film as a nanoscale mask for creating the polymer nanowires array. Put the Au-coated FEP into inductively coupled plasma (ICP) chamber, and introduce O<sub>2</sub>, Ar, and CF<sub>4</sub> gases into the ICP chamber at flow rates of 10.0, 15.0, and 30.0 sccm, respectively. Use one power source of 400 W to generate a large density of plasma and another power source of 100 W to accelerate plasma ions toward the FEP surface. And then perform the ICP reactive ion etching for 60 s. The surface morphology of the FEP thin film was characterized by a Hitachi SU-8010.

### Gas sensing materials synthesis and characterization

The rhombus-shaped Co<sub>3</sub>O<sub>4</sub> nanorod arrays were prepared via a two-step fluorine-mediated hydrothermal process [6,13]. All chemicals or materials were of analytical grade and used directly without any further purification prior to usage. Deionized water (18.3 M $\Omega$  cm) was produced by using a Millipore Direct-Q System, and used throughout the experiments. The typical synthesis was carried out at a temperature of 95 °C for 12 h and characterized by X-ray diffraction (XRD), scanning electron microscopy (SEM).

### Electrical measurement

Acquire the output voltage signal of the BD-TENG via a voltage preamplifier (Keithley 6514 System Electrometer) and the output current signal by a low-noise current preamplifier (Stanford Research System SR570). The software platform is constructed based on LabView, which is capable of realizing real-time data acquisition control and analysis.

### Gas-sensing measurement

The electrical characteristics were measured at room temperature in the dark using a semiconductor parameter analyzer (Agilent E5270B) with the bias voltage range of  $-10$  to 10 V. The gas-sensing properties were performed in a high vacuum system (Lacotech, LVS-1P2703) with a volume of 50 L, as shown in Fig. S1. The gas sensor was driven by the BD-TENG under different blowing speeds. When the output was stable, saturated target gas was injected into the test chamber by a micro-injector through a rubber plug. The saturated target gas was mixed with air (relative humidity was  $\sim 40\%$ ). After the output reached a new constant value, the test chamber was opened to recover the sensors in air. The voltage and current were acquired and analyzed by the system in real time. Gas response was designated as the ratio  $V_a/V_g$ , where  $V_g$  is the voltage of a mixture of target gas while  $V_a$  is in air. Response and recovery time are defined as the time needed for 90% of total resistance change on exposure to gas and air, respectively.

## Results and discussion

The basic structure of the BD-TENG mainly consists of three functional parts: a rotator, a stator and a soft elastic, as

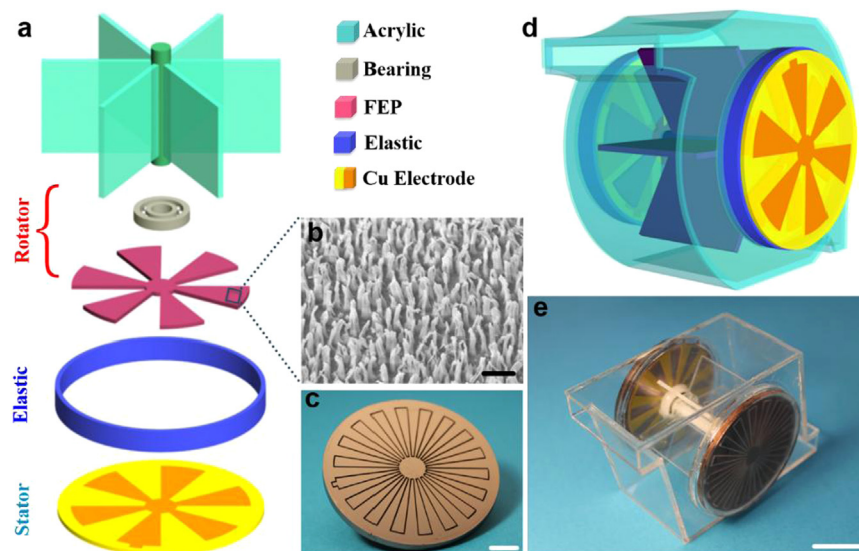


**Fig. 1** Device structure of the blow-driven triboelectric nanogenerator (BD-TENG). (a) Schematic illustrations of the functional components of BD-TENG, which mainly consists of three parts, a rotator, a stator and a soft elastic. (b) A SEM image of the FEP polymer nanowires (scale bar, 500 nm). (c) A photograph of the as-fabricated stator (scale bar, 1 cm). (d) A schematic illustration of the BD-TENG and (e) a photograph of an as-fabricated BD-TENG (scale bar, 2cm).

schematically illustrated in Fig. 1(a). And the rotator can be further decomposed into three parts: a rotor blade to convert the air flow into a rotation, a disk made of acrylic with a layer of FEP at the top, and a bearing to connect the two. Photographs of the as-fabricated three components are respectively shown in Fig. S2(a)-(c). The FEP layer is  $\sim 50 \mu\text{m}$  in thickness and 5 cm in diameter, which was patterned into radially arrayed sectors with each sectional angle of  $10^\circ$ . And then it was aligned onto the acrylic disk surface. Nanowire structures were created on the exposed FEP surface by a top-down method through ICP etching to enhance the triboelectrification for an enhanced electric output. A SEM image of the vertically aligned FEP nanowires is displayed in Fig. 1(b), which indicates that the average clustering diameter of FEP nanowires is  $\sim 100 \text{ nm}$  with an average length of  $\sim 1 \mu\text{m}$ . The stator is composed of two copper electrodes with complementary patterns, which have been separated by fine trenches in between, as shown in Fig. 1(c). The soft elastic is made of sponge, which acts as a spacer between the FEP layer and the Cu thin film, a photograph of the spacer is shown in Fig. S2(d). Fig. 1(d) is a sketch of the as-developed breath analyzer with two vent ports for air flowing. And the photograph of an as-fabricated device is shown in Fig. 1(e).

The working principle of the as-developed alcohol sensor is schematically depicted in Fig. 2, which could be elaborated from two aspects, one is the air blowing induced electricity generation part, which is the TENG, and the other is the alcohol adsorption-desorption induced resistance change, which is the sensor part that is electrically driven by the TENG for gas measurements.

The electricity generation of the BD-TENG is based on the coupling between contact electrification and electrostatic induction [25-28]. The working principle of a sector unit is depicted in Fig. 2(a). Here, both three-dimensional schematic illustrations of the rotation states (up) and their corresponding two-dimensional potential distribution (down) were used for

illustration. To start, an external pressure, e.g. finger taping, will bring the rotator to contact with the stator. The FEP on the rotator will thus contact with the copper foil on the stator. Due to a different electron affinities of the two, charge transfer emerges at the interface and the electron will inject from copper to FEP [29-32]. When the pressure was released, the soft elastic will separate the two. However, the generated triboelectric charges are non-mobile and could sustain on the surfaces. Here, the initial state and the final state are respectively the states when the rotator is aligned with the electrode 1 and electrode 2. And the intermediate state represents the transitional process in which the stator spins away from the initial state to the final state. At the initial state, the FEP fully aligns with the electrode 1, which corresponds to a maximum electrical potential on electrode 1 and a minimum potential on the electrode 2, and thus a maximized electrical potential difference between the two, namely, a maximized open-circuit voltage. When the rotator starts to spin as driven by the blowing air, the open-circuit voltage starts to diminish till the middle point, where it turns to zero. Further rotation beyond this point will result in a reversely established open-circuit voltage and is maximized at the final state [33-35]. This is a full cycle of the voltage generation process. To obtain a quantitative understanding about the working mechanism, numerical calculations on the induced potential difference in different motion steps were also carried out using COMSOL (Fig. S3).

When an external resistive sensor is applied, the voltage drop applied over the load by the BD-TENG increases with increasing the load resistance of a sensor. This trend can be used for self-powered active gas sensing if the magnitude of the resistance is tunable via controlling the gas concentration at the vicinity of the sensor. Regarding the alcohol sensor, a p-type  $\text{Co}_3\text{O}_4$  was synthesized that exhibiting a resistance increasing upon an increasing of the ambient alcohol concentration. The driving force of this trend is presented in Fig. 2(b). In vacuum, the main charge carriers of  $\text{Co}_3\text{O}_4$  are holes. After being

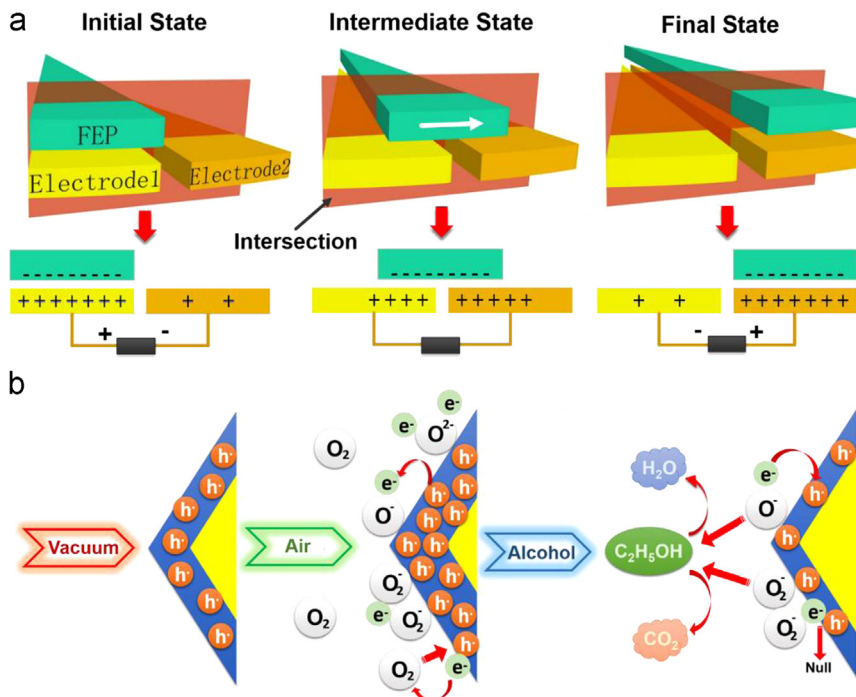


**Fig. 2** Working principle of the BD-TENG for self-powered gas sensing. (a) An illustration of electricity generation process of the BD-TENG, which holds three states, the initial state, intermediate state and final state. (b) Schematic diagram of the chemical reactions under the applied voltage generated by the BD-TENG for self-powered gas sensing. And the proposed chemical reaction process was described as three states, respectively, the surface processes in vacuum, air and alcohol vapor atmosphere.

exposed to air, the surface of  $\text{Co}_3\text{O}_4$  is readily covered with negatively charged chemisorbed oxygen ( $\text{O}^-$ ,  $\text{O}^{2-}$  and  $\text{O}_2^-$ ) [36,37]. As a result, an increasing of the conductivity emerges due to the generated holes and the thus formed charge accumulation layer on the surface. Then, when the alcohol is introduced, the charge carrier accumulation layer near the surface is thinned by the electrochemical interaction between negatively charged chemisorbed oxygen and ethanol molecules, which releases free electrons and neutralizes the generated holes [38,39]. The resistance is thus increased until a dynamic equilibrium is re-established. A coupling of the  $\text{Co}_3\text{O}_4$  resistance change with the blow-driven triboelectric nanogenerator as the power source, a novel active alcohol gas sensor was thus developed.

To characterize the electric output of the BD-TENG, the measurement was performed under different wind speeds. As shown in Fig. 3(a), the open circuit voltage holds almost constant at various wind speeds. While the output current shows a positively proportional relationship with the wind speeds, as demonstrated in Fig. 3(b). This is because the output voltage depends on the maximum mismatched area of the two triboelectric layers in the TENG, while the current depends on the speed at which the sliding occurs. The presented BD-TENG was driven by mouth blowing for an active alcohol detection, which requires the electric output signal is independent of the wind speeds for an accurate calibration. To evaluate the resistance dependent electric output, external load was applied, as shown in Fig. 3(c). The output voltage increases with load resistance while the output current exhibits an opposite trend. Both curves have a quasi-linear region between 0.1 and 100 M $\Omega$ . Inset is the circuit for performing the measurement. Fig. 3(d) plots the current-voltage ( $I$ - $V$ )

characteristics between the two neighboring electrodes bridged by the gas-sensing materials. The current increased linearly with applied bias, which indicates a good ohmic contact between the two. And this linear  $I$ - $V$  curve ensures that all of the upcoming gas sensing behaviors can be fully captured and exhibited from the corresponding curve change [40,41]. The up-left inset is the SEM image of the  $\text{Co}_3\text{O}_4$  nanorod arrays, which holds a rhombic shape with an average edge length of 400 nm (Fig. S4(a) and (b)). The down-right inset is the sketch of the gas sensor for alcohol adsorption. The corresponding XRD pattern and Raman spectrum of the as-synthesized  $\text{Co}_3\text{O}_4$  are presented in Fig. S4(c) and (d).

To characterize the performance of the BD-TENG based active alcohol sensor, the first step was to determine the optimum working temperature for the sensor. As shown in Fig. 4 (a), under a fixed alcohol concentration of 100 ppm, the voltage was found to increase with the operating temperature, and then decrease with a further increase, which indicates an optimized working temperature of the sensor tip is at 160 °C for the alcohol sensing system. It is unfortunate that this part of heating energy has to be supplied by a power source. Furthermore, the output characteristic of the BD-TENG at the optimized working temperature of 160 °C was also systematically investigated. As shown in Fig. 4(b) and (c), the voltage and current output varies with alcohol concentrations in a range of 10 to 2000 ppm. For TENG, when the load resistance range is from 100  $\Omega$  to 0.1 M $\Omega$ , the voltage increases with increasing the load resistance, while the current output holds almost constant in such range. The real-time resistance change of the  $\text{Co}_3\text{O}_4$  based gas sensor is shown in Fig. S5, which indicates a resistance change range of 0.2 to 7 k $\Omega$  at 160 °C with an applied 100 ppm alcohol. When the alcohol

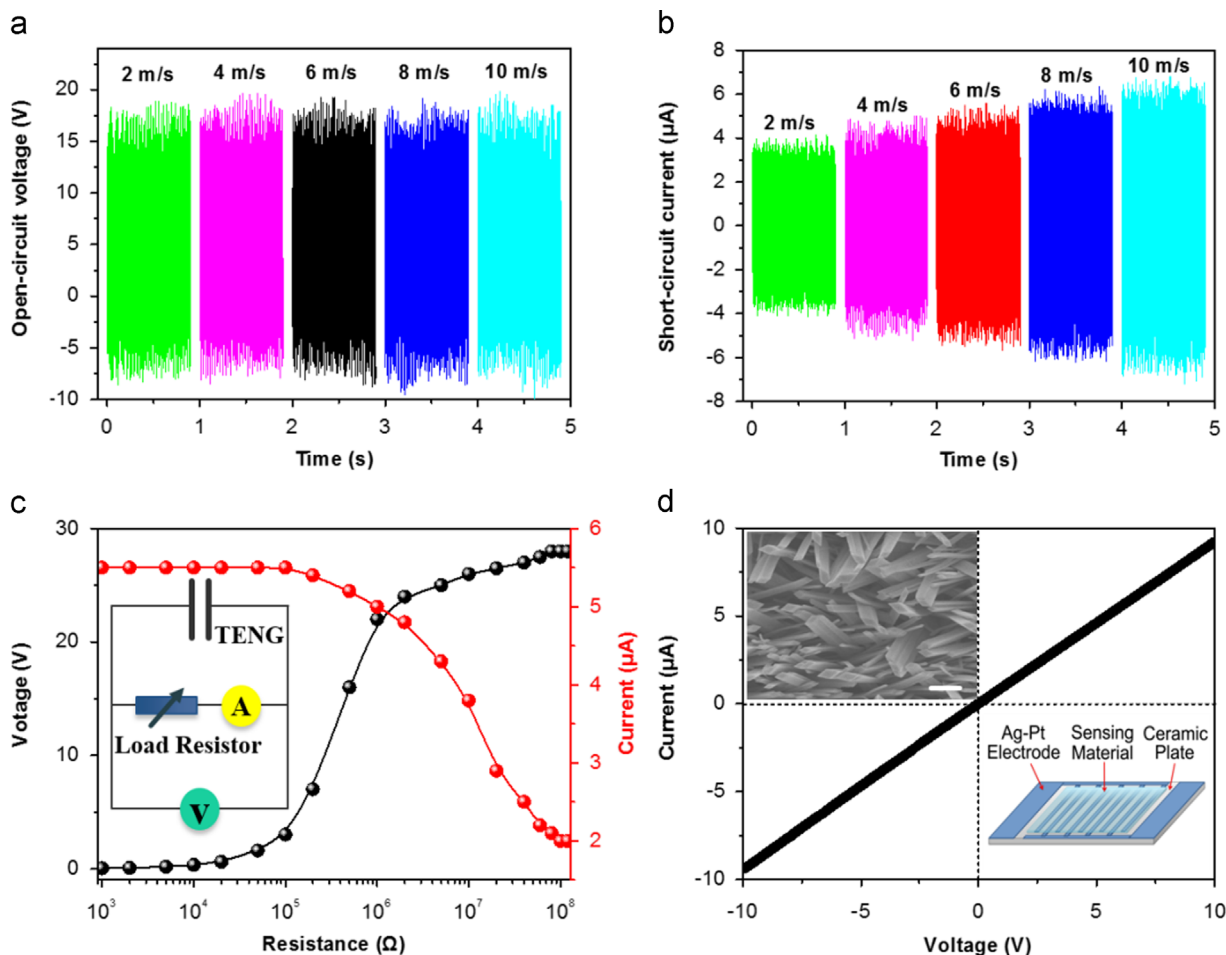


**Fig. 3** Electrical output characterizations of the BD-TENG. Dependence of the (a) open-circuit voltage and (b) short-circuit current on various blowing speeds from 2 to 10 m/s. (c) The variation of the output voltage and current with external load resistances under a fixed blowing speed of 6 m/s (Inset is the measurement circuit diagram). (d) The current-voltage ( $I$ - $V$ ) curve of the as-fabricated alcohol sensor. The up-left inset shows a SEM image of the synthesized rhombus-shaped  $\text{Co}_3\text{O}_4$  nanorod arrays. The scale bar is 500 nm. And the down-right inset shows the structural design of the alcohol sensor.

concentrations increase, the resistance of the  $\text{Co}_3\text{O}_4$  based gas sensor also increases accordingly. Consequently, the voltages increase with the increasing alcohol concentrations while the current output holds almost constant. An enlarged view of the voltage without alcohol is demonstrated in Fig. S6. Moreover, the result indicates that the BD-TENG based gas sensor could detect ethanol in a wide range of concentrations with a low detection limitation of 10 ppm. Fig. 4(d) displays the measured gas response curve of the as-developed breath analyzer in term of voltage with a testing range of 10–2000 ppm at a working temperature of 160 °C. At the lower concentration range below 200 ppm, the voltage increases linearly with the elevated alcohol concentration. While at a higher concentration range of above 500 ppm, a saturation emerges due to the fully adsorbed positions. Inset is the enlarged view of the response curve in a range of 10 to 200 ppm, which confirms capability of the device for low concentration alcohol detection. Fig. 4(e) is a real-time continuously measured voltage profile to show the dynamic response of the BD-TENG to ambient alcohol concentrations, which renders a fast response and recovery time of 11 and 20 s, respectively. It proves that the approach is an effective way for

rapid alcohol detection. Fig. 4(f) shows the selectivity of the BD-TENG as an active gas sensor for alcohol detection. The gas response to 100 ppm alcohol vapor is  $\sim 34.5$ , which is significantly higher than other similar gases, including isopropanol ( $\sim 23.2$ ), methanol ( $\sim 18.6$ ), acetone ( $\sim 6.3$ ) and toluene ( $\sim 1.8$ ), under the same concentration. This test exhibits high anti-interference ability of the device for alcohol detection.

To demonstrate, the BD-TENG was integrated with a signal-processing circuit to develop a complete wireless warning system. The circuit diagram of the complete self-securing system is shown in Fig. S7. And a photograph of the customized signal processing circuit was shown in Fig. S8. It is worth noting that, for an experimental demonstration, here we employed a heating platform to assure a normal working temperature of 160 °C for the sensor. When the BD-TENG was blew by a tester without drinking alcohol, the voltage drop across the sensor is almost zero due to a low sensor resistance (Fig. 5(a)). When the BD-TENG was blew by a tester after alcohol drinking, the breathed-out alcohol vapor will dramatically increase the resistance of the sensor, which leads to an increased voltage drop across the sensor, as shown in Fig. 5(b). This increased

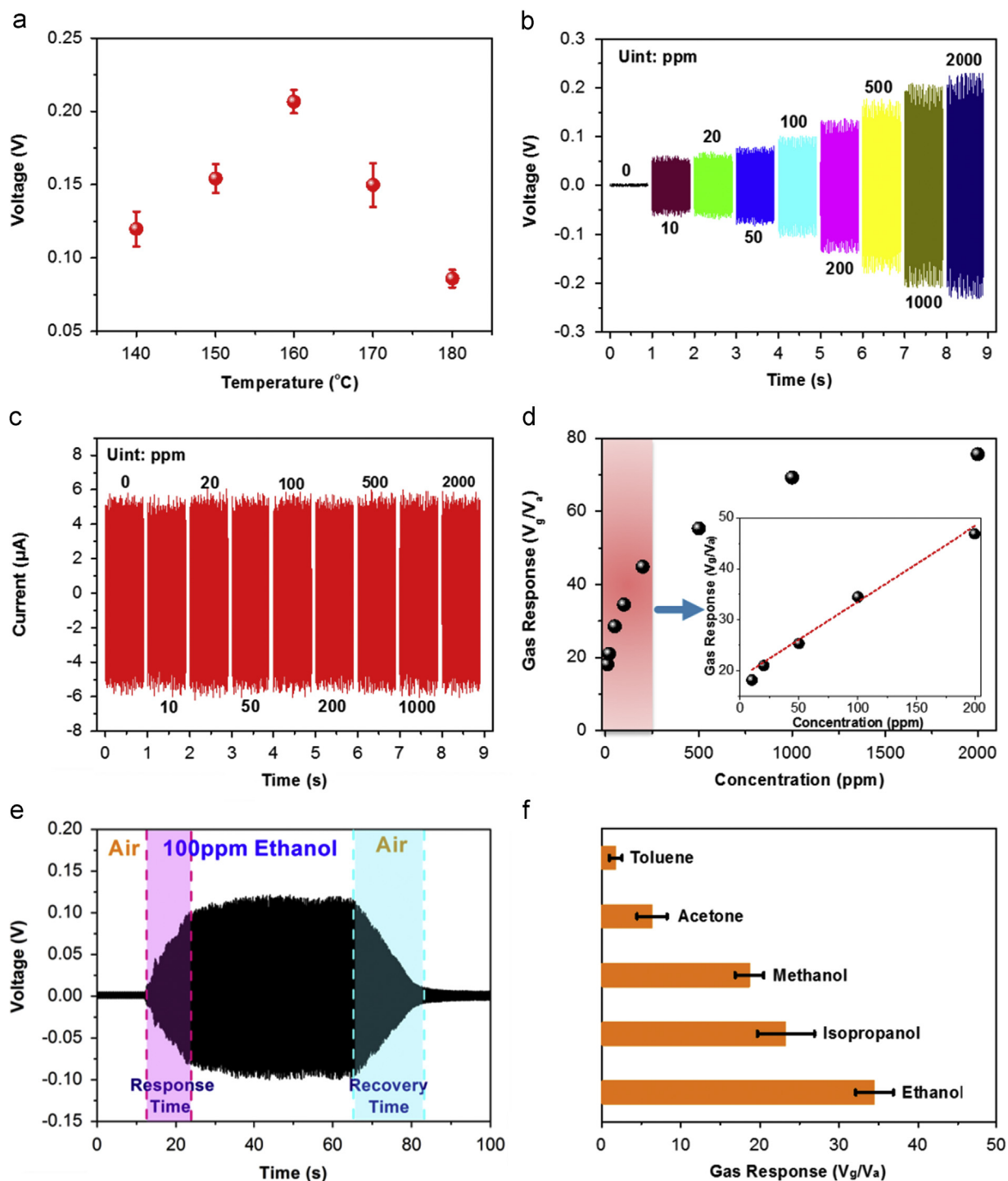


**Fig. 4** Performance characterization of the self-powered alcohol sensor based on a BD-TENG. (a) Under a fixed alcohol concentration of 100 ppm, the dependence of the voltage output on the applied temperatures, which indicates an optimized working temperature of 160  $^{\circ}\text{C}$ . Under a fixed temperature of 160  $^{\circ}\text{C}$ , the variation of (b) output voltage and (c) current with alcohol concentrations ranging from 10 to 2000 ppm. (d) The measured gas response curve in term of output voltage. Inset is the enlarged view of the response curve in a range of 10 to 200 ppm. (e) A real-time continuously measured voltage profile to show the dynamic response of the BD-TENG to ambient alcohol concentrations. (f) Test of the selectivity of the BD-TENG based self-powered alcohol sensor.

voltage signals trigger an IC timer that controls a wireless transmitter and remotely switches a siren between a panic state and a silence state. Fig. 5(c) is a schematically illustration of the BD-TENG based wireless warning system for the alcohol

drunk test. And Fig. 5(d) is a photograph of the corresponding experimental setup. As shown, when a person after drinking alcohol blew the BD-TENG, the siren will be on with light flashing as a warning (Movie S1).

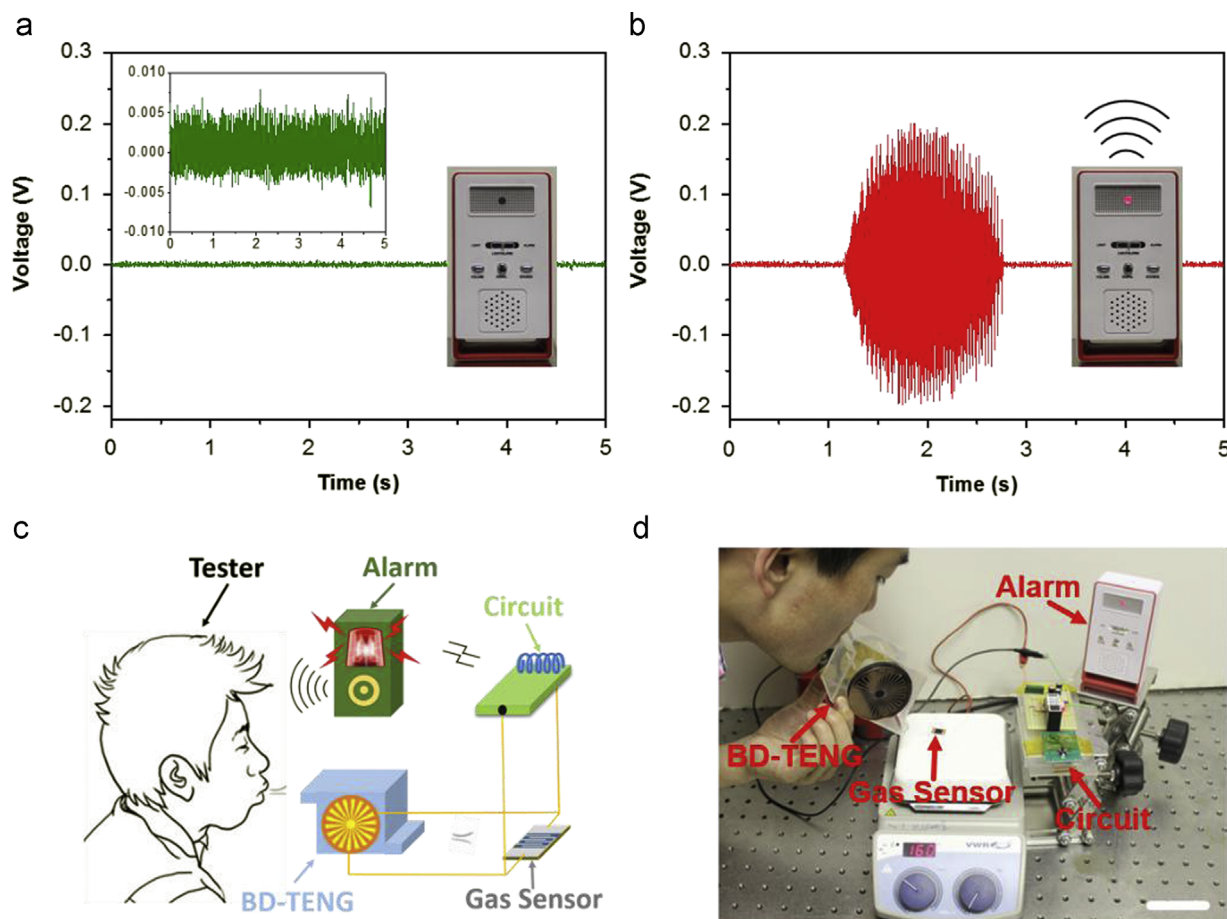


**Fig. 5** Demonstration of the BD-TENG as a self-powered breath analyzer. The acquired voltage signals of the BD-TENG when it was blew by a tester (a) before and (b) after drinking alcohol. The insets show that a wireless alarm was triggered with siren on after drinking alcohol. (c) A schematic illustration and (d) a photograph showing the BD-TENG acting as a self-power breath analyzer. The scale bar is 5 cm.

The BD-TENG based alcohol breath analyzer holds several unique advantages. First, the output voltage is independent of the blowing speed and also the user. The constant output voltage of the BD-TENG is exceptional for the alcohol detection. Second, the voltage is sensitive to the external resistance in a range of 0.1 and 100 M $\Omega$ , and this tunable resistance is easy to be fulfilled by various alcohol concentrations. Third, a designed trigger voltage threshold of 0.1 V enables the alcohol breath analyzer to work stably even when the gas concentration is very low.

## Conclusion

In this work, we introduced a fundamentally new working principle in the gas sensing field by fabricating a blow-driven triboelectric nanogenerator (BD-TENG) that supplies the power for the sensor measurement. By using a mouth blowing, the induced output voltage is constant and independent of the users and blowing speed. But it holds a proportional relationship with the breathed-out alcohol concentration. The response to 100 ppm vapor ethanol reached  $\sim 34$  with low detection limit of 10 ppm. Meanwhile, the sensor exhibited good response/recovery kinetics (11 s and 20 s) and also outstanding

selectivity anti-interference ability. When a drinking person blew the BD-TENG gently, the generated voltage signals can trigger to emit a warning signal. We must point out that although the TENG can supply the power for the sensor measurement, the power required for the heating unit has to be supplied. In a case we can find materials that works good for gas sensing at room temperature, such a sensor is truly totally self-powered. Given other competitive features, including being light-weight, easy fabrication, cost effectiveness, the justified concept in this work not only launches a new approach with extensive potential in the field of gas sensing, but also make a significant progress towards the practical application of TENGs as self-powered active sensors.

## Acknowledgements

Z. W., J. C. and M.-H. Y. contributed equally to this work. The research was supported by Hightower Chair foundation, and the National High Technology Research and Development Program ("863"Program) of China (2015AA034801). Z.W. would also like to acknowledge the fellowship from the China Scholarship Council (CSC). M.-H. Y. thanks the support from Ministry of Science and Technology, Taiwan (MOST 103-2917-I-564-070).

The Patents have been filed based on the research results presented in this manuscript.

## Appendix A. Supporting information

Supplementary data associated with this article can be found in the online version at <http://dx.doi.org/10.1016/j.nanoen.2015.06.006>.

## References

- [1] M.W. Hoffmann, L. Mayrhofer, O. Casals, L. Caccamo, F. Hernandez-Ramirez, G. Lilienkamp, W. Daum, M. Moseler, A. Waag, H. Shen, J.D. Prades, *Adv. Mater.* 26 (2014) 8017-8022.
- [2] X. Han, M. Jin, S. Xie, Q. Kuang, Z. Jiang, Y. Jiang, Z. Xie, L. Zheng, *Angew. Chem. Int. Ed. Engl.* 48 (2009) 9180-9183.
- [3] P. Offermans, M. Crego-Calama, S.H. Brongersma, *Nano Lett.* 10 (2010) 2412-2415.
- [4] H.-J. Kim, J.-H. Lee, *Sens. Actuators, B: Chem.* 192 (2014) 607-627.
- [5] A. Tricoli, M. Righettoni, A. Teleki, *Angew. Chem. Int. Ed. Engl.* 49 (2010) 7632-7659.
- [6] Z. Wen, L. Zhu, W. Mei, Y. Li, L. Hu, L. Sun, W. Wan, Z. Ye, *J. Mater. Chem. A* 1 (2013) 7511-7518.
- [7] Z.-H. Lin, G. Cheng, W. Wu, K.C. Pradel, Z.L. Wang, *ACS Nano* 8 (2014) 6440-6448.
- [8] H. Zhang, Y. Yang, Y. Su, J. Chen, C. Hu, Z. Wu, Y. Liu, C. Ping Wong, Y. Bando, Z.L. Wang, *Nano Energy* 2 (2013) 693-701.
- [9] A.K. Wanekaya, M. Uematsu, M. Breimer, O.A. Sadik, *Sens. Actuators, B: Chem.* 110 (2005) 41-48.
- [10] S. Sanze, A. Gurlo, C. Hess, *Angew. Chem. Int. Ed. Engl.* 52 (2013) 3607-3610.
- [11] M.C. Janzen, J.B. Ponder, D.P. Bailey, C.K. Ingison, K. S. Suslick, *Anal. Chem.* 78 (2006) 3591-3600.
- [12] K.-C. Kim, S.M. Cho, H.-G. Choi, *Sens. Actuators, B: Chem.* 67 (2000) 194-198.
- [13] Z. Wen, L. Zhu, Z. Zhang, Z. Ye, *Sens. Actuators, B: Chem.* 208 (2015) 112-121.
- [14] J. Chen, G. Zhu, J. Yang, Q. Jing, P. Bai, W. Yang, X. Qi, Y. Su, Z.L. Wang, *ACS Nano* 9 (2015) 105-116.
- [15] J. Chen, J. Yang, Z. Li, X. Fan, Y. Zi, Q. Jing, H. Guo, Z. Wen, K.C. Pradel, S. Niu, Z.L. Wang, *ACS Nano* 9 (2015) 3324-3331.
- [16] G. Zhu, J. Chen, Y. Liu, P. Bai, Y.S. Zhou, Q. Jing, C. Pan, Z.L. Wang, *Nano Lett.* 13 (2013) 2282-2289.
- [17] X. Fan, J. Chen, J. Yang, P. Bai, Z. Li, Z.L. Wang, *ACS Nano* 9 (2015) 4236-4243.
- [18] J. Yang, J. Chen, Y. Su, Q. Jing, Z. Li, F. Yi, X. Wen, Z. Wang, Z.L. Wang, *Adv. Mater.* 27 (2015) 1316-1326.
- [19] J. Yang, J. Chen, Y. Yang, H. Zhang, W. Yang, P. Bai, Y. Su, Z.L. Wang, *Adv. Energy Mater.* 4 (2014) 1301322.
- [20] W. Yang, J. Chen, X. Wen, Q. Jing, J. Yang, Y. Su, G. Zhu, W. Wu, Z.L. Wang, *ACS Appl. Mater. Interfaces* 6 (2014) 7479-7484.
- [21] Z. Li, J. Chen, J. Yang, Y. Su, X. Fan, Y. Wu, C. Yu, Z.L. Wang, *Energy Environ. Sci.* 8 (2015) 887-896.
- [22] T.-C. Hou, Y. Yang, H. Zhang, J. Chen, L.-J. Chen, Z.L. Wang, *Nano Energy* 2 (2013) 856-862.
- [23] H. Guo, J. Chen, M.H. Yeh, X. Fan, Z. Wen, Z. Li, C. Hu, Z.L. Wang, *ACS Nano* 9 (2015) 5577-5584.
- [24] Z.H. Lin, G. Zhu, Y.S. Zhou, Y. Yang, P. Bai, J. Chen, Z.L. Wang, *Angew. Chem. Int. Ed. Engl.* 52 (2013) 5065-5069.
- [25] W. Yang, J. Chen, G. Zhu, J. Yang, P. Bai, Y. Su, Q. Jing, X. Cao, Z.L. Wang, *ACS Nano* 7 (2013) 11317-11324.
- [26] Y. Su, J. Chen, Z. Wu, Y. Jiang, *Appl. Phys. Lett.* 106 (2015) 013114.
- [27] J. Chen, G. Zhu, W. Yang, Q. Jing, P. Bai, Y. Yang, T.C. Hou, Z.L. Wang, *Adv. Mater.* 25 (2013) 6094-6099.
- [28] G. Zhu, B. Peng, J. Chen, Q. Jing, Z.L. Wang, *Nano Energy* 14 (2015) 126-128.
- [29] W. Yang, J. Chen, G. Zhu, X. Wen, P. Bai, Y. Su, Y. Lin, Z.L. Wang, *Nano Res.* 6 (2013) 880-886.
- [30] G. Zhu, P. Bai, J. Chen, Z.L. Wang, *Nano Energy* 2 (2013) 688-692.
- [31] J. Yang, J. Chen, Y. Liu, W. Yang, Y. Su, Z.L. Wang, *ACS Nano* 8 (2014) 2649-2657.
- [32] W. Yang, J. Chen, Q. Jing, J. Yang, X. Wen, Y. Su, G. Zhu, P. Bai, Z.L. Wang, *Adv. Funct. Mater.* 24 (2014) 4090-4096.
- [33] G. Zhu, J. Chen, T. Zhang, Q. Jing, Z.L. Wang, *Nat. Commun.* 5 (2014) 3426.
- [34] L. Lin, S. Wang, S. Niu, C. Liu, Y. Xie, Z.L. Wang, *ACS Appl. Mater. Interfaces* 6 (2014) 3031-3038.
- [35] P. Bai, G. Zhu, Y. Liu, J. Chen, Q. Jing, W. Yang, J. Ma, G. Zhang, Z.L. Wang, *ACS Nano* 7 (2013) 6361-6366.
- [36] Z. Wen, L. Zhu, Y. Li, Z. Zhang, Z. Ye, *Sens. Actuators, B: Chem.* 203 (2014) 873-879.
- [37] W.Y. Li, L.N. Xu, J. Chen, *Adv. Funct. Mater.* 15 (2005) 851-857.
- [38] L. Zhang, Z. Gao, C. Liu, Y. Zhang, Z. Tu, X. Yang, F. Yang, Z. Wen, L. Zhu, R. Liu, Y. Li, L. Cui, *J. Mater. Chem. A* 3 (2015) 2794-2801.
- [39] Z. Wen, L. Zhu, W. Mei, L. Hu, Y. Li, L. Sun, H. Cai, Z. Ye, *Sens. Actuators, B: Chem.* 186 (2013) 172-179.
- [40] M.W. Ahn, K.S. Park, J.H. Heo, J.G. Park, D.W. Kim, K.J. Choi, J.H. Lee, S.H. Hong, *Appl. Phys. Lett.* 93 (2008) 263103.
- [41] Z. Wen, L. Zhu, L. Li, L. Sun, H. Cai, Z. Ye, *Dalton Trans.* 42 (2013) 15551-15554.



**Zhen Wen** received his B.S. in Materials Science and Engineering from China University of Mining and Technology (CUMT) in 2011. He started to pursue his Ph.D. degree at Zhejiang University (ZJU) after that. Now he is a visiting Ph.D. student at Georgia Institute of Technology through the program of China Scholarship Council (CSC). His research interests mainly focus on nano-materials and nano-energy.

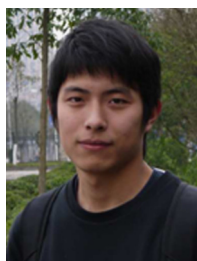


**Jun Chen** received the B.S. and M.S. in Electrical Engineering from the School of Electronic Information and Communications at Huazhong University of Science and Technology in 2007 and 2010, respectively, and a second M.S. in Biological Engineering from the College of Engineering at The University of Georgia in 2012. He is currently a Ph.D. candidate in the School of Materials Science and Engineering at the Georgia Institute of Technology, working

under the guidance of Prof. Zhong Lin Wang. His research focuses primarily on nanomaterial-based energy harvesting, energy storage, active sensing and self-powered micro-/nano-systems. His H-index is 22.



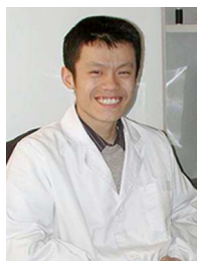
**Min-Hsin Yeh** received his Ph.D. in Chemical Engineering from National Taiwan University (NTU) in 2013 under the supervision of Prof. Kuo-Chuan Ho. Now he is a visiting scholar at Prof. Zhong Lin Wang's group in the school of Materials Science and Engineering, Georgia Institute of Technology. His research interests mainly focus on triboelectric nanogenerator, self-powered electrochemical systems, electrochemistry, sensitized solar cells, and other energy materials.



**Hengyu Guo** received his B. S. in Applied Physics from Chongqing University, China in 2012. He is a Ph.D. candidate with the research focus on Condensed Matter Physics, Chongqing University. And now he is a visiting Ph.D. student at Georgia Institute of Technology through the program of China Scholarship Council (CSC). His current research interest is energy harvesting for self-powered systems.



**Zhaoling Li** is a Ph. D. candidate in the College of Textiles in Donghua University, China. He is currently a visiting student in the School of Materials Science and Engineering at Georgia Institute of Technology under the supervision of Prof. Zhong Lin (Z. L.) Wang. His research mainly focuses on triboelectric nanogenerators as sustainable power sources and self-powered active sensing.



**Xing Fan** received his Ph.D. from Peking University in 2009. He then joined the College of Chemistry and Chemical Engineering of Chongqing University. Now he is a visiting scholar at Georgia Institute of Technology through the program of China Scholarship Council. His current research interests include electrochemistry and nano energy.



**Tiejun Zhang** got his bachelor degree in 1982 from Northeastern University in China. After graduation, he has over 20 years experiences as an EM service engineer and EM Lab engineer, and performed the installation, calibration, teaching, operation, cost-effective preventive maintenance and repair-trouble shooting of advanced microscopy and materials characterization instrumentation and sample preparation equipment.



**Dr. Liping Zhu** received her B.S. (1988) and M.S. (1991) in Materials Science from Zhejiang University, and a Ph.D from the Hiroshima University in Japan in 2002. After that, she joined the Materials Department of Zhejiang University. Her current research interests include semiconductor materials, photo-electronic thin films, nano-materials and their applications in gas sensing, energy storage, photocatalysis, solar cell.



**Dr. Zhong Lin Wang** is a Hightower Chair and Regents's Professor at Georgia Tech. He is also the Chief scientist and Director for the Beijing Institute of Nanoenergy and Nanosystems, Chinese Academy of Sciences. His discovery and breakthroughs in developing nanogenerators establish the principle and technological road map for harvesting mechanical energy from environmental and biological systems for powering personal electronics. His research on self-powered nanosystems has inspired the worldwide effort in academia and industry for studying energy for micro-nano-systems, which is now a distinct disciplinary in energy research and future sensor net works. He coined and pioneered the field of piezotronics and piezo-phototronics by introducing piezoelectric potential gated charge transport process in fabricating new electronic and optoelectronic devices. This historical breakthrough by redesigning CMOS transistor has important applications in smart MEMS/NEMS, nanorobotics, human-electronics interface and sensors.